(Received 16 September 2025, Accepted 15 October 2025, Scheduled 24 October 2025)

A Miniaturized Balanced Bandpass Filter with Biaxial Symmetry Using C-Section Parallel-Coupled Microstrip Lines

Chuan Shao[1,*], Xin Gao[2], Rong Cai[1], Xinnai Zhang[1], and Kai Xu[3]

[1]*Nantong Key Laboratory of Artificial Intelligence New Quality Technology Jiangsu College of Engineering and Technology, Nantong 226000, Jiangsu, China*
[2]*Shanghai Institute of Satellite Engineering, Shanghai 201109, China*
[3]*Nantong Key Laboratory of Advanced Microwave Technology, Nantong University, Nantong 226019, Jiangsu, China*

ABSTRACT: In this paper, a miniaturized balanced bandpass filter characterized by biaxial symmetry is designed and implemented using four C-section parallel-coupled microstrip lines. As two orthogonal symmetric axes are inherently embedded across the filter layout, a natural geometric constraint is imposed and therefore furnishes two independent input/output port states. Owing to its symmetric topology, the developed filter replicates the same differential- and common-mode responses at each of its two independent input/output port pairs. To further enhance the common-mode suppression without compromising the differential-mode performance, a quarter-wavelength open-circuited stub is introduced onto the junction of one of the C-section parallel-coupled microstrip lines. By utilizing this stub, the common-mode suppression bandwidth is effectively broadened. Moreover, highly compact circuit sizes are achieved for the developed balanced filters, which is regarded as essential for their integration into modern miniaturized microwave communication systems. Finally, the feasibility of the proposed concept is verified through the design and fabrication of two prototypes, and good agreement is observed between the simulated and measured results.

1. INTRODUCTION

Nowadays, balanced filters are widely studied for their critical role in suppressing common-mode noise and preserving differential-mode responses. Their performance has been intensively improved to meet the ever-stricter electromagnetic-compatibility regulations imposed by modern high-speed systems. Furthermore, significant research effort has been devoted to extending balanced-filter theory, as superior common-mode rejection is continuously demanded for next-generation wireless and wireline applications [1–6].

Over the past few years, many architectures and methodologies have been proposed for balanced bandpass filters (BPFs). Accordingly, almost every common transmission line structure, such as microstrip lines [7–9], waveguides [10–13], striplines [14], etc. [15–17], has been employed to design these filters. Moreover, schemes that combine different transmission lines have been introduced, and the common-mode suppression of the resulting balanced BPFs has been improved by approaches such as integrating microstrip lines with slotlines [18–20].

Balanced filters realized using microstrip lines are widely favored [7–9], as their geometry is perceived to be simple, their fabrication cost is kept low, and they are easily integrated with active devices. Meanwhile, stripline-based balanced filters are now massively deployed, driven by the rapid advances in low temperature co-fired ceramic multilayer processes [14]. Based on microstrip and stripline, balanced BPFs are generally designed using half-wavelength or quarter-wavelength resonators. However, these two types of transmission lines are usually suitable for lower frequency bands. Moreover, stripline structure cannot be easily connected to active devices like microstrip. At higher frequencies, balanced filters that are constructed with waveguide structures, including several recently reported substrate integrated waveguide structures, are preferred because high unloaded Q factors are maintained well into the millimeter wave range [10–13]. Nevertheless, balanced filters based on waveguide structures are often relatively large in size, which may limit their application in compact and integrated systems.

In the differential-fed BPFs described above, the input and output ports are assigned to a fixed pair of terminals, and this single choice automatically fixes the geometric symmetric plane [1–6]. If those terminals are later driven with reversed polarity, the resulting differential- and common-mode responses no longer coincide with the original ones, because the symmetric plane has been effectively reversed.

In this paper, a miniaturized balanced BPF formed by four C-section parallel coupled microstrip lines is presented. Two orthogonal symmetric axes are embedded in the layout, so the symmetric plane can be oriented either horizontally or vertically while the same differential-mode passband and common-mode rejection are preserved in both orientations, which has rarely been mentioned in earlier balanced filters. Accordingly, two independent input and output port assignments are created by these two orthogonal axes, and an additional degree of free-

* Corresponding author: Chuan Shao (ch_shao@jcet.edu.cn).

dom is provided to the designer without any alteration of the electrical response.

2. OPERATING PRINCIPLES OF THE PROPOSED BALANCED BPFS

2.1. Analysis of the Original Structure

The transmission line model of the proposed balanced BPF is depicted in Fig. 1. As presented in the figure, the developed balanced BPF is constituted by four C-section of parallel-coupled microstrip lines with electrical length of θ and two pairs of differential-fed ports. Benefitting from its exactly mirrored layout, the proposed filter is mirror-symmetric with respect to both the x-axis and y-axis, hereafter referred to as plane I and plane II. Owing to the biaxial symmetry (BS) of the structure, the differential- and common-mode equivalent circuits obtained with plane I and plane II as symmetric planes are identical. Therefore, only the analysis with plane I as the symmetric plane is presented here.

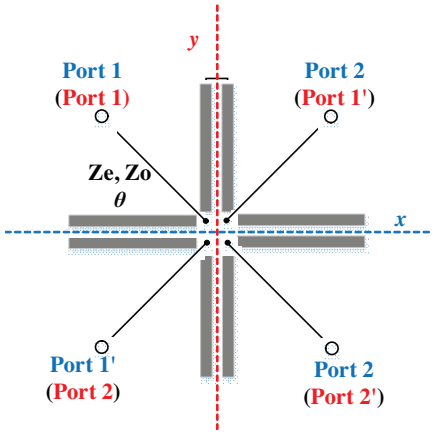

FIGURE 1. Transmission line model of the proposed balanced BPF with BS.

When plane I is taken as the plane of symmetry, the proposed balanced BPF is subjected to odd-even mode analysis. The resulting differential- and common- mode equivalent circuits, as shown in Fig. 2, are both symmetric with respect to the dashed line.

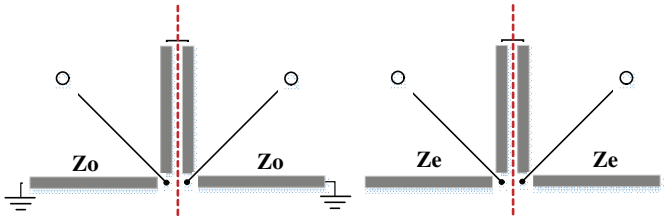

FIGURE 2. Differential-mode and common-mode equivalent circuits of the proposed balanced BPF with BS.

Subsequently, an additional odd-even-mode analysis is performed on the aforementioned differential-mode bisection. As a result, odd-mode and even-mode equivalent circuits for the differential-mode bisection are respectively illustrated in Fig. 3. For the odd-mode equivalent circuit of the differential-mode bisection, its input admittance is given by:

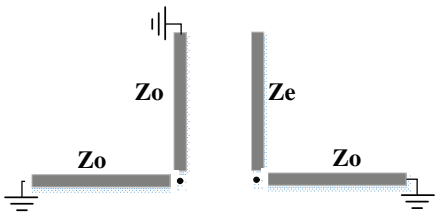

FIGURE 3. Odd-mode and even mode equivalent circuits for the differential-mode bisection.

$$Y_{inDMo} = \frac{2}{jZ_o \tan\theta} \tag{1}$$

When Y_{inDMo} is set to zero, the resonance frequency of the equivalent circuit is fixed at $\pi/2$, and a transmission pole is created exactly at the center frequency f_0 in the differential-mode response.

The input admittance of the even-mode equivalent circuit, which corresponds to the differential-mode equivalent circuit, is expressed as:

$$Y_{inDMe} = \frac{1}{jZ_o \tan\theta} - \frac{1}{jZ_e \cot\theta} \tag{2}$$

Based on the established link between S_{dd11} and the odd- and even-mode input admittances (Y_{inDMe} and Y_{inDMo}) for the differential-mode responses [21], the expression below is derived:

$$S_{dd11} = \frac{Y_0^2 - Y_{inDMe}Y_{inDMo}}{(Y_0 + Y_{inDMe})(Y_0 + Y_{inDMo})} \tag{3}$$

By imposing the condition $S_{dd11} = 0$, another two transmission poles (θ_{p1}, θ_{p2}) for the differential mode are identified and can be expressed as follows:

$$\theta_{p1} = \arctan\left(\sqrt{\frac{2Z_eZ_0^2}{2Z_oZ_0^2 - Z_o^2Z_e}}\right) \tag{4}$$

$$\theta_{p2} = \pi - \theta_{p1} \tag{5}$$

where Z_0 is the characteristic impedance of the input and output ports.

In the common-mode equivalent circuit depicted in Fig. 2, the C-section parallel-coupled structure demonstrates an all-pass response characteristic [22]. The two open-circuit stubs located on either side of this structure function as quarter-wavelength open-circuited stubs for the input and output ports, thereby generating a transmission zero for the common-mode responses at the center frequency for the differential mode.

Simulated differential- and common-mode responses of the developed balanced filter for various combinations of Z_o and Z_e are depicted in Fig. 4 and Fig. 5. As shown in these figures, the simulated results align well with the previous theoretical predictions. A transmission zero in the common-mode response is precisely located at the center frequency of the differential-mode response, and the common-mode response

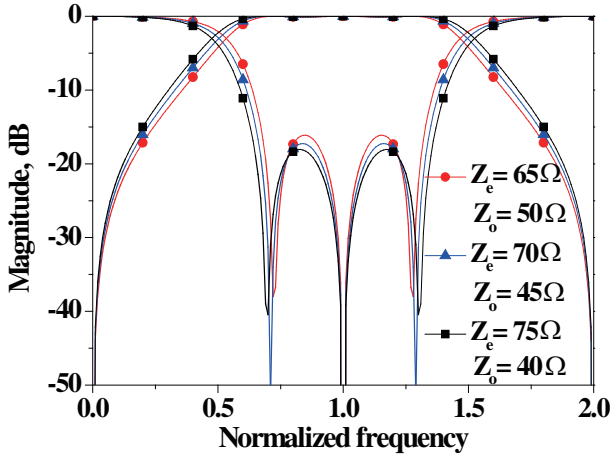

FIGURE 4. Differential-mode responses of the original structure.

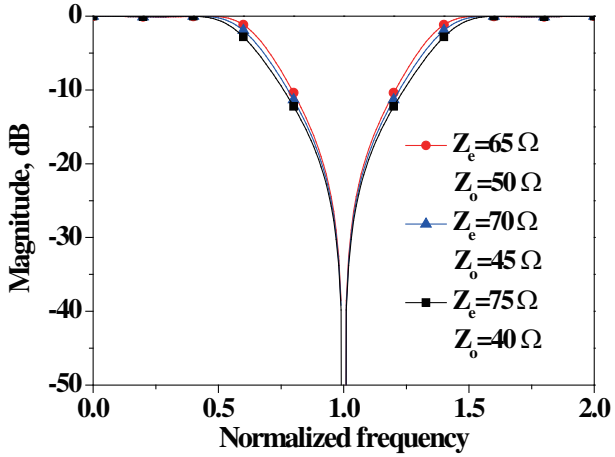

FIGURE 5. Common-mode responses of the original structure.

remains essentially unchanged for all considered combinations of Z_o and Z_e. In addition, as can be seen from Fig. 4, with the increase of the coupling coefficient $C = (Z_e - Z_o)/(Z_e + Z_o)$, the working bandwidth of the differential-mode passband also increases.

2.2. Analysis of the Modified Structure

To further enhance the common-mode suppression for the original structure, the previously described balanced filter is refined. The structure of the modified structure is illustrated in Fig. 6. Specifically, an open-circuit stub, characterized by a length of θ and a characteristic impedance of $2Z_1$, is incorporated onto the junction of one of the utilized C-section parallel-coupled microstrip lines.

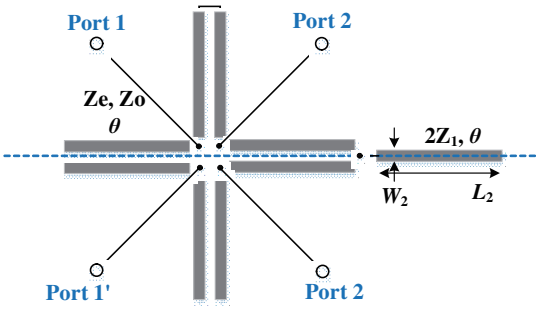

FIGURE 6. Transmission line model of the modified structure.

Given that the additional open-circuit stubs do not alter the differential-mode equivalent circuit of the modified balanced filter when considering the dashed line in Fig. 6 as the plane of symmetry, the differential-mode equivalent circuit remains identical to that of the original structure. Consequently, further elaboration on the differential-mode analysis is deemed unnecessary.

The common-mode equivalent circuit in Fig. 7 is similar to the common-mode equivalent circuit in Fig. 2 in that the C-section parallel-coupled structure exhibits an all-pass response. The open-circuit stub on the left side effectively generates a transmission zero precisely at the center frequency for the differential mode. This is because the input impedance of the

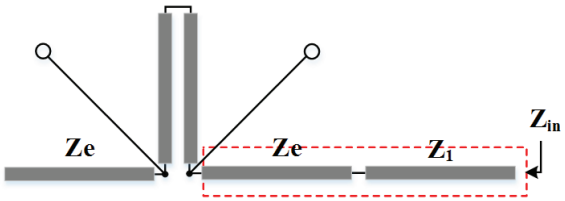

FIGURE 7. Common-mode equivalent circuit for the modified balanced filter.

open-circuit stub equals zero, resulting in a solution of $\pi/2$ [23]. Accordingly, the transmission zeros generated by the structure enclosed by the dashed box in Fig. 7 can also be derived using the same method. The input impedance of the structure enclosed by the dashed box in Fig. 7 can be obtained as:

$$Z_{ins} = jZ_1 \frac{Z_1 \tan^2\theta - Z_e}{(Z_e + Z_1)\tan\theta} \tag{6}$$

According to [24], by imposing the condition $Z_{in} = 0$, the locations of the transmission zeros introduced by this structure can be readily determined. Solving $Z_{in} = 0$ yields the two transmission zeros as:

$$\theta_{Z1} = \arctan\sqrt{\frac{Z_e}{Z_1}} \tag{7}$$

$$\theta_{Z2} = \pi - \theta_{Z1} \tag{8}$$

To verify the theoretical analysis and the derived formulas, common-mode responses for the modified balanced filter versus Z_1 are presented in Fig. 8. As can be seen from Fig. 8, while keeping the odd- and even-mode impedances constant, the positions of the two additional transmission zeros can be adjusted merely by varying the value of Z_1. In this way, specific common-mode frequencies within the differential-mode operating band can be suppressed simply by tuning the value of Z_1.

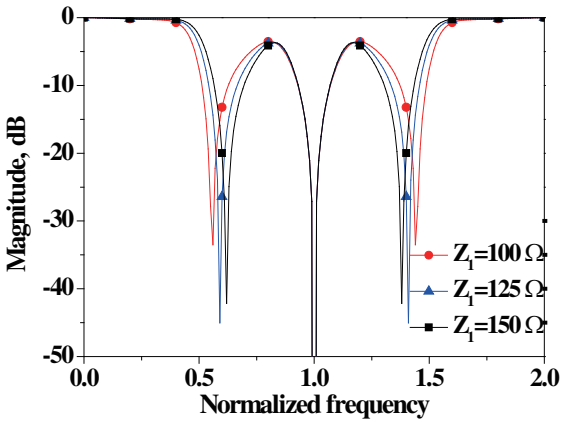

FIGURE 8. Common-mode responses for the modified balanced filter versus Z_1. ($Z_e = 70\,\Omega$, $Z_o = 45\,\Omega$).

3. RESULTS AND DISCUSSIONS

Based on the foregoing analysis, odd- and even-mode characteristic impedances of 45 Ω and 70 Ω are selected to guarantee the desired performance for the developed balanced filter. Additionally, the center frequency of the differential mode is determined to be 3 GHz, and the substrate employed is Rogers 4003c (a loss tangent of 0.0027, a dielectric constant of 3.55, and a thickness of 0.508 mm). The layout and photograph of the proposed balanced BPF with BS are given in Fig. 9 and Fig. 10, respectively.

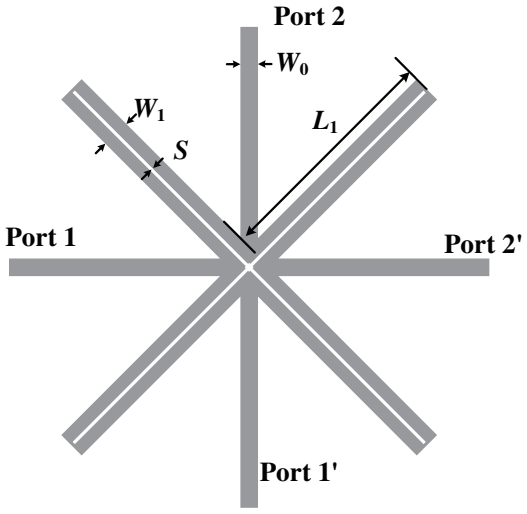

FIGURE 9. Layout of the proposed balanced BPF with BS ($W_0 = 1.15$ mm, $W_1 = 1.8$ mm, $L_1 = 14.8$ mm, $S = 0.2$ mm).

The simulation and measurement for the proposed balanced BPF are accomplished using a full-wave simulator Ansys HFSS 2020 R2 and a Keysight 5230C four-port vector network analyzer, respectively. To verify the port-scheme independence, one differential-fed pair is arbitrarily constituted by selecting any two adjacent ports, while the remaining two ports are assigned as another differential-fed pair. Accordingly, the corresponding measurement-to-simulation comparison is then presented in Fig. 11. In Fig. 11, Sdd21 represents the differential-mode transmission from port 1 to port 2; Sdd11 represents

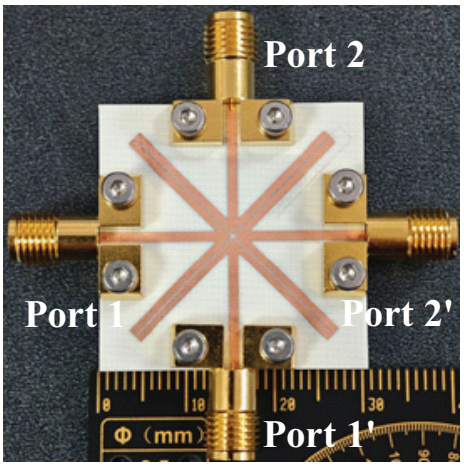

FIGURE 10. Photograph of the proposed balanced BPF with BS.

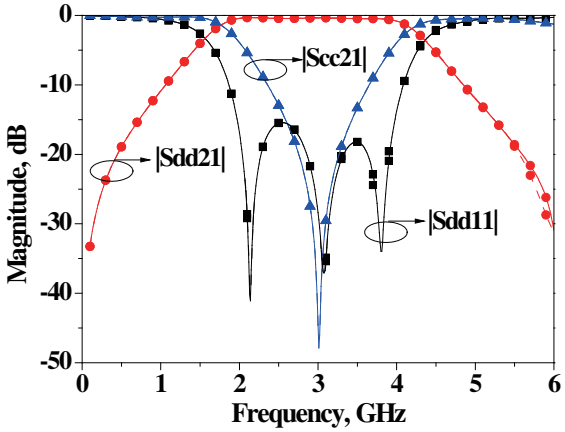

FIGURE 11. Simulated and measured results of the developed balanced BPF. (Simulated results: dashed lines, measured results: solid lines).

the differential-mode reflection at port 1; and Scc21 represents the common-mode transmission from port 1 to port 2. It can be observed from the figure that the center frequency of the differential-mode response of the filter is 3 GHz, with a 1-dB passband bandwidth of 2.4 GHz, corresponding to a relative bandwidth of 80%. Within the 1-dB differential-mode bandwidth, common-mode signals are suppressed to varying degrees, with the maximum level of suppression exceeding 45 dB.

In order to further enhance the common-mode rejection bandwidth for the proposed balanced filter, a quarter-wavelength open-circuited stub has been loaded onto the junction of one of the utilized C-section parallel-coupled microstrip lines, whose photograph is shown in Fig. 12, and the simulated and measured results are plotted in Fig. 13. According to Fig. 13, with the open-circuited stub added, the open-circuited stub introduces two additional transmission zeros in the common-mode transmission coefficient, located on either side of the original three transmission zeros, while the differential-mode response remains essentially unchanged. Benefiting from these two extra transmission zeros introduced by the open circuited stub, the 5 dB common mode rejection band is widened from 2.08 to 3.93 GHz to 1.71 to 4.35 GHz,

TABLE 1. Comparison with previously reported balanced BPFs.

Ref.		f_0 GHz/*FBW*	Insertion loss, dB	Process	CM* suppression level and bandwidth	Size $\lambda_g \times \lambda_g$	Flexible I/O ports
7		1.95/24%	2.93	MSL	40 dB (DC ~ 4 GHz)	0.75 × 0.65	NO
8		5.7/12%	0.85	MSL	34 dB (4 ~ 9 GHz)	NA	NO
9		0.725/12%	3.2	MSL	45 dB (0.375 ~ 1 GHz)	NA	NO
10		2.5/20%	0.37	WG	60 dB (DC ~ 9 GHz)	0.44 × 0.22	NO
11		3.5/15.8%	1.93	WG	37 dB (14 ~ 20 GHz)	NA	NO
12		3.5/13%	0.35	WG	60 dB (DC ~ 6 GHz)	3.75 × 1.8×	NO
13		3/15.8%	3.07	SIW	41 dB (1.5 ~ 4.5 GHz)	NA	NO
14		2.45	2.4	SL	38 dB (1 ~ 4 GHz)	0.12 × 0.1	NO
15		3/5.8%	1.55	DSPSL	25 dB (DC ~ 9 GHz)	1 × 0.88	NO
16		1.17/3.4%	0.45	CL	60 dB (1 ~ 2 GHz)	NA	NO
17		2/87%	0.85	CPS	39 dB (DC ~ 5 GHz)	1.9 × 0.3	NO
18		4/35%	1.36	MSL-SL	44 dB (2 ~ 6 GHz)	NA	NO
19		5.75/93%	0.5	MSL-SL	33 dB (2 ~ 10 GHz)	NA	NO
20		2/70%	1.2	MSL-SL	35 dB (DC ~ 5 GHz)	0.93 × 0.48	NO
This works	Original structure	3/80%	0.3	MSL	5 dB (2.08 ~ 3.93 GHz)	0.37 × 0.37	YES
	Modified structure				5 dB (1.71 ~ 4.35 GHz)	0.4 × 0.37	NO

* CM stands for common-mode.

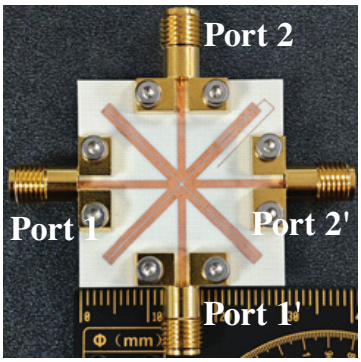

FIGURE 12. Photograph of the modified structure of the balanced filter in Fig. 10 ($L_2 = 15.1$ mm, $W_2 = 0.1$ mm).

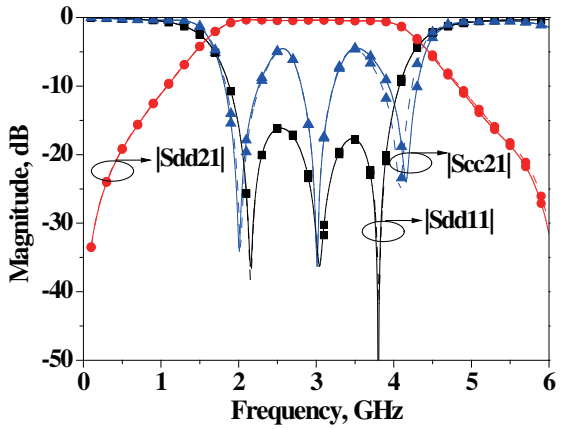

FIGURE 13. Simulated and measured results of the modified structure of the balanced filter in Fig. 10. (Simulated results: dashed lines, measured results: solid lines).

an enhancement of roughly 43%, while the overall circuit area is hardly increased. More importantly, the locations of these two transmission zeros can be accurately shifted by merely adjusting the characteristic impedance of the added stub, thereby enabling selective suppression of common-mode signals at any specified frequency inside the differential pass-band.

Table 1 presents a comparison of the proposed balanced BPFs with previously reported balanced BPFs, based on microstrip line (MSL), waveguide (WG) including substrate-integrated waveguide (SIW), stripline (SL), double-sided parallel-strip line (DSPSL), coaxial line (CL), coplanar strip line (CPS), and hybrid microstrip-slotline (MSL-SL) structures. According to this table, it can be seen that previously reported balanced filters based on various transmission lines have exhibited good differential-mode responses and satisfactory common-mode suppression. However, all these structures possess only one symmetric plane, so the input and output ports are fixed and cannot be made flexible, as enabled by the original structure proposed in this work.

4. CONCLUSION

In this study, a miniaturized wideband balanced bandpass filter has been initially proposed, which is characterized by biaxial symmetry. Owing to two orthogonal symmetric axes built into the layout, the filter naturally offers two distinct, interchangeable input/output port configurations. Moreover, in either configuration, the circuit preserves a wide differential-mode pass-

band while strongly suppressing common-mode noise. To further elevate common-mode rejection, a quarter-wavelength open-circuited stub is loaded at the junction of one C-shaped parallel coupled microstrip section which introduces two additional transmission zeros in the common-mode response. Measured results closely follow simulated predictions, validating both the design procedure and the practical feasibility of the proposed balanced filter.

ACKNOWLEDGEMENT

This work was supported by the National Natural Science Foundation of China under Grants 62201291, Natural Science Research Project of Jiangsu Higher Education Institutions (Grant 23KJD510002, 25KJB420002), and Natural Science and Technology Project of Jiangsu College of Engineering and Technology (Grant GYKY/2024/5, JSGYZRJJZD-03).

REFERENCES

[1] Martin, F. and F. Medina, "Balanced microwave transmission lines, circuits, and sensors," *IEEE Journal of Microwaves*, Vol. 3, No. 1, 398–440, Jan. 2023.

[2] Feng, W., W. Che, and Q. Xue, "New balance-applications for dual-mode ring resonators in planar balanced circuits (application notes)," *IEEE Microwave Magazine*, Vol. 20, No. 7, 15–23, Jul. 2019.

[3] Arbelaez-Nieto, A., E. Cruz-Perez, J.-L. Olvera-Cervantes, A. Corona-Chavez, and H. Lobato-Morales, "The perfect balance-a design procedure for balanced bandpass filters [application notes]," *IEEE Microwave Magazine*, Vol. 16, No. 10, 54–65, Nov. 2015.

[4] Feng, W., W. Che, and Q. Xue, "The proper balance: Overview of microstrip wideband balance circuits with wideband common mode suppression," *IEEE Microwave Magazine*, Vol. 16, No. 5, 55–68, Jun. 2015.

[5] Zhang, S. T., H. R. Zhang, and W.-T. Li, "Differential filtering quad-band antenna based on enhanced folded-dipole," *Progress In Electromagnetics Research C*, Vol. 150, 9–16, 2024.

[6] Zhao, X.-B., F. Wei, L. Yang, and R. Gómez-García, "Two-layer-magic-T-based bandpass, quasi-bandstop, and dual-passband balanced filters with differential-/common-mode reflectionless behavior," *IEEE Transactions on Microwave Theory and Techniques*, Vol. 72, No. 4, 2267–2282, Apr. 2024.

[7] Zhang, Z., G. Zhang, Z. Liu, W. Tang, and J. Yang, "Compact balanced bandpass filter based on equilateral triangular patch resonator," *IEEE Transactions on Circuits and Systems II: Express Briefs*, Vol. 69, No. 1, 90–93, Jan. 2022.

[8] Wei, F., Y.-C. Xue, X.-B. Zhao, W.-S. Liu, L. Xu, and P. F. Zhang, "Balanced bpf with dual-port quasi-reflectionless characteristic and selectivity enhancement," *IEEE Transactions on Circuits and Systems II: Express Briefs*, Vol. 70, No. 3, 994–998, Mar. 2023.

[9] Simpson, D., P. Vryonides, S. Nikolaou, and D. Psychogiou, "Non-reciprocal balanced bandpass filters with quasi-elliptic response," *IEEE Transactions on Circuits and Systems II: Express Briefs*, Vol. 69, No. 12, 5159–5163, Dec. 2022.

[10] Zhang, C.-Y., X. Shi, Y.-H. Zhu, Y. Xue, and J.-X. Chen, "A compact interlaced-double-ridge waveguide balanced filter with wideband CM suppression," *IEEE Microwave and Wireless Technology Letters*, Vol. 35, No. 2, 169–172, Feb. 2025.

[11] Chen, J.-X., Y. Xue, X. Shi, Y.-X. Huang, W. Qin, and Y.-J. Yang, "Design of double-ridge waveguide balanced filter and filtering power divider," *IEEE Transactions on Microwave Theory and Techniques*, Vol. 72, No. 10, 5929–5937, Oct. 2024.

[12] Wei, F., X.-C. Zhou, Z.-H. Shi, H.-Y. Liu, and P.-Y. Qin, "A balanced bandpass filter with high-selectivity and common-mode suppression based on inverted microstrip gap waveguide," *IEEE Microwave and Wireless Technology Letters*, Vol. 35, No. 2, 181–184, Feb. 2025.

[13] Xie, W.-B., Y.-H. Ma, D.-W. Wang, C.-H. Yu, Y. Hu, and W.-S. Zhao, "Compact single-and dual-band balanced high-selectivity bandpass filters based on microstrip resonator loaded substrate integrated waveguide," *IEEE Transactions on Electromagnetic Compatibility*, 2025.

[14] Chen, J.-X., C. Shao, Q.-Y. Lu, H. Tang, and Z.-H. Bao, "Compact LTCC balanced bandpass filter using distributed-element resonator," *Electronics Letters*, Vol. 49, No. 5, 354–356, Feb. 2013.

[15] Xue, Y.-C., F. Wei, Q. Li, and X.-Z. Ding, "Arbitrary-order balanced BPFs and common-and differential-mode quasi-reflectionless BPFs using out-of-phase coupled DSPSL," *IEEE Transactions on Microwave Theory and Techniques*, Vol. 73, No. 5, 2879–2891, May 2025.

[16] Lu, Q.-Y., W. Qin, and J.-X. Chen, "A novel balanced bandpass filter based on twin-coaxial resonator," *IEEE Microwave and Wireless Components Letters*, Vol. 27, No. 2, 114–116, Feb. 2017.

[17] Ouyang, Z.-A., L. Zhu, and L.-L. Qiu, "Wideband balanced filters with intrinsic common-mode suppression on coplanar stripline-based multimode resonators," *IEEE Transactions on Circuits and Systems I: Regular Papers*, Vol. 69, No. 6, 2263–2275, Jun. 2022.

[18] Li, Z., F. Wei, B. Liu, and X. W. Shi, "Design of balanced wideband BPF based on tri-mode slotline resonators," *IEEE Transactions on Circuits and Systems II: Express Briefs*, Vol. 69, No. 6, 2767–2771, Jun. 2022.

[19] Zhao, X.-B., F. Wei, M. Malki, L. Yang, and R. Gómez-García, "Planar balanced quadruplet bandpass filter with extended common-and differential-mode two-port quasi-reflectionless ranges," *IEEE Microwave and Wireless Technology Letters*, Vol. 34, No. 1, 25–28, Jan. 2024.

[20] Yang, L. and R. Gómez-García, "High-order quasi-elliptic-type single-ended and balanced wideband bandpass filters using microstrip-to-microstrip vertical transitions," *IEEE Transactions on Circuits and Systems II: Express Briefs*, Vol. 70, No. 4, 1425–1429, Apr. 2023.

[21] Zhu, L., S. Sun, and R. Li, *Microwave Bandpass Filters for Wideband Communications*, John Wiley & Sons, 2011.

[22] Pozar, D. M., *Microwave Engineering: Theory and Techniques*, John Wiley & Sons, 2021.

[23] Gao, X., "Investigations on novel microwave wideband passive filtering circuits," Ph.D. dissertation, Nanjing University of Science and Technology, Nanjing, China, 2020.

[24] Gao, X., W. Feng, W. Che, and Q. Xue, "Wideband balanced-to-unbalanced filtering power dividers based on coupled lines," *IEEE Transactions on Microwave Theory and Techniques*, Vol. 65, No. 1, 86–95, Jan. 2017.